

Strategy to Antibacterial, High-Mechanical, and Degradable Poly(lactic acid)/Chitosan Composite Film through Reactive Compatibilization via Epoxy Chain Extender

Tingqiang Yan, Xiaodong Wang, and Yingjie Qiao*

Cite This: *ACS Omega* 2024, 9, 27312–27320

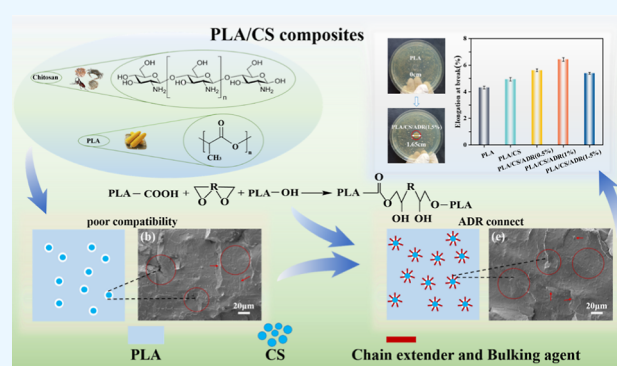
Read Online

ACCESS |

Metrics & More

Article Recommendations

ABSTRACT: Research into the production of antibacterial, high strength, and environmentally friendly biobased films for use in food packaging is crucial due to growing concerns about food safety. Herein, the preparation of antibacterial, high mechanical, and degradable Poly(lactic acid)/chitosan (PLA/CS) composite films with exceptional interfacial compatibility through reactive compatibilization via the epoxy chain extender ADR4468 is reported. A strong bond, in the form of a chemical bond between PLA and CS, is established by the cycloaddition opening reaction of ADR, which induces cross-linking between hydroxyl and carboxyl groups on the molecular chains. As a result, the elongation at break increased by 31.8% compared to the composite film without ADR. In addition, the composite films exhibited good compost degradability, with a mass reduction of 42–45% after 100 days of degradation.



1. INTRODUCTION

In today's world, there is an increasing demand for film materials due to the improvement in people's living standards. Film materials are used to meet daily production and life needs, effectively enhancing people's quality of life. Among these materials, antimicrobial food packaging is designed to extend shelf life and inhibit the growth of microorganisms, ensuring food quality and safety.^{1,2} Most film materials used today are made from nonbiodegradable plastics. These plastics do not decompose naturally and must be discarded or incinerated at high temperatures after use. This can result in global warming, water pollution, and air pollution.³ In addition, waste incineration at high temperatures produces significant amounts of carbon dioxide that diffuse into the air, contributing to global warming and the greenhouse effect.⁴ Due to the growing severity of global 'white pollution' and the gradual depletion of oil resources, there is an increasing focus on biodegradable materials. Therefore, it is imperative to conduct research on biodegradable film materials.⁵ The challenge for the plastics and polymer composites industry is to replace commodity plastics of petrochemical origin with biobased polymers or recyclable and environmentally sustainable composites. This is necessary to address environmental concerns and reduce the need to recycle synthetic polymer waste.^{6–8} Poly(lactic acid) (PLA) is a biodegradable material made from plant starch. It is environmentally friendly, has high tensile strength and hardness, and has excellent processing

properties. Furthermore, it is fully biodegradable under composting conditions after disposal.⁹

Recent innovations in manufacturing processes for agricultural monomers have significantly reduced the cost of producing PLA. As a result, PLA has expanded its end use from biomedical materials to commodity plastics, such as food packaging films.¹⁰ PLA has been chosen as an alternative to nonbiodegradable plastic films because of its availability, biodegradability, and good food contact properties. Despite the many advantages of PLA, its poor gas barrier properties, low toughness and ductility, and poor thermal stability still limit its applications, such as injection molding (blown film or blow molding).^{11,12} Several advances have been made in PLA modification today, including copolymerization, blending, compounding, and the addition of modifiers to PLA and other substances to improve their related properties.

Studies have shown that modification of PLA with epoxy chain expanders to obtain long branched structures is an effective way to improve the mechanical properties of PLA, epoxy chain extenders are versatile, thermally stable, and easy

Received: February 26, 2024

Revised: April 13, 2024

Accepted: June 4, 2024

Published: June 12, 2024



to obtain properties that can reconnect the cleaved chains by increasing the molecular weight and melt strength of the polymer and can also be used as reactive compatibilizers in blends.^{13,14} Epoxy chain extenders can react with the end groups $-OH$ and $-COOH$ of PLA to form high molecular weight polymers.¹⁵ Sun et al.¹⁶ used ADR epoxy chain extender to toughen PLA in the molten state. Arruda et al. used the chain extender ADR-4370F to prepare PLA/PBAT films by blow molding and used them in food packaging.¹⁷ Highly environmentally friendly PLA-based biodegradable materials are proven for their use with polymers of natural origin, fully biodegradable and sustainable biopolymers [including starch, cellulose, natural fibers, chitin and chitosan (CS), collagen, lignin, natural rubber, polyhydroxy fatty acid esters, soy-based resins, etc.]. Composites that do not generate hazardous waste at the end of their life cycle.^{18–20}

Meanwhile, a certain percentage of CS is introduced into the PLA-based food packaging film for better food preservation. CS has excellent antibacterial activity and biodegradability. Studies have shown that CS has good antibacterial properties in PLA-based composite films and can improve the film-forming ability of composite films.²¹ Moreover, due to its natural origin and excellent properties, such as biodegradability, biocompatibility, and nontoxicity, it has been widely used in several industries.^{22–28} Bie et al.²⁹ added a certain amount of CS to PLA starch to develop antibacterial PLA/ST/CS composites by the melt extrusion process. The material has effective and long-lasting antibacterial properties against *Escherichia coli* and *Staphylococcus aureus*. Therefore, the addition of CS to food packaging films is of great significance for food preservation.

In this work, we introduced CS to enrich the bacteriostatic properties of PLA films and used the chain-expanding property of ADR to enhance the interfacial compatibility of the composite films by chemically bonding CS and PLA, resulting in the preparation of a thermodynamically compatible PLA/CS composite film. This study could provide a reference for the development of PLA-based composite films.

2. MATERIALS AND METHOD

2.1. Materials. PLA, model 4032D, produced by Nature Work, USA. CS, degree of deacetylation 98%, was produced by Aladdin, USA. The chain extender ADR4468, food grade, was produced by BASF, Germany.

2.2. Preparation of Composite Film. Adoption of the multifunctional food-grade epoxy chain extender ADR4468. On the basis of maintaining the ratio of PLA to CS at 96:4, three ratios of 0.5, 1, and 1.5% of ADR4468 were introduced into it, as shown in Table 1. The PLA/CS/ADR composite film was obtained by melt blending and chain expansion using a twin-screw extruder (Twin-screw machine, SHJ20, Nanjing Jainte Mechatronics Co) and thermocompression molding

(Hot Press, BL6170, Dongguan Baolun Precision Instrument Co) using a hot press. Testing of the composite films: the specific steps are drying PLA in an oven at 80 °C for 12 h, drying CS in an oven at 105 °C for 12 h, drying food grade epoxy chain extender ADR4468 in a vacuum oven at 60 °C for 8 h, and dispersing PLA, CS, and ADR4468 every 1 h to make them completely dry. After drying the raw materials, PLA, CS, and ADR4468 were weighed and mixed well by hand in the following proportions (Table 1), then melt and comingle extrusion was carried out using a twin-screw extruder. The extrusion temperature was set to 135–160–180–180–135 °C for each range from the inlet to the outlet. The homogeneously mixed PLA/CS/ADR mixture was crushed in a multifunctional pulverizer. Finally, the obtained PLA/CS/ADR mixture was ground and then hot pressed at 180 °C under 8 MPa pressure for 5 min under a hot press for compression molding, and the PLA/CS/ADR composite film was obtained with a film thickness of 0.2 mm. The name of the composite film was defined by the amount of ADR added to the composite film, i.e., when the amount of ADR added was 0.5%, the name of the composite film was PLA/CS/ADR (0.5%) composite film, and so on, as follows.

2.3. Fourier Transform Infrared Spectroscopy. The chemical structure of PLA-based composite films was characterized by Fourier transform infrared spectroscopy (FTIR spectrometer, Tensor, Bruker, Germany). Thirty-two scans were performed with a wavenumber range of 500–4000 cm^{-1} and a resolution of 4 cm^{-1} .

2.4. Mechanical Properties. According to the GB1040.3-2006 method for the composite film stretching test (Mechanical Experiment Machine, CMT5504, Shenzhen New Sansi Testing Co), the stretching speed was set to 5 mm/min, each group of samples was tested 7 times in parallel, the maximum and minimum values were removed, and the average value and deviation were calculated as the measurement results.

2.5. Contact Angle Measurement. An OCA20 contact angle measuring instrument was used to test the contact angle of the PLA-based composite film surface (contact angle tester, OCA20, DATA PHYSICS, Germany). The composite film was placed flat on the sample table, deionized water was selected as the test solution at room temperature, the volume of water droplets was set to 4 μL , and the test time was 20 s.

2.6. Water Absorption Rate. According to GB1034-98, the PLA-based composite films were cut into three 25 × 25 mm sizes, placed in a drying oven at 60 °C for 72 h, and then removed and weighed (recorded as m_1). The film was soaked in a beaker with 300 mL of distilled water, and the water was removed and wiped off the surface every 72 h, and weighed again (recorded as m_2). The average value was calculated and recorded until the water absorption (WA) of the composite film reached saturation. WA was calculated according to eq 1.

$$\text{WA} = (m_2 - m_1)/m_1 \times 100\% \quad (1)$$

2.7. Water Vapor Permeability. The thickness of the PLA-based composite film was measured with a vernier caliper (noted as X) in accordance with ASTM E96-1995. 2 g of anhydrous calcium chloride were added to the test glass vial, at which time the relative humidity in the test glass vial (noted as RH₂) was 0. The test glass vial was sealed with the PLA-based composite film, weighed, and placed the glass vial in a desiccator with a saturated NaCl solution at the bottom (at which time the temperature was maintained at 25 °C and the

Table 1. Raw Material Ratio of PLA/CS/ADR Composite Film

sample	PLA (wt %)	CS (wt %)	ADR (wt %)
PLA	100	0	0
PLA/CS	96	4	0
PLA/CS/0.5ADR	95.5	4	0.5
PLA/CS/1.0ADR	95	4	1
PLA/CS/1.5ADR	94.5	4	1.5

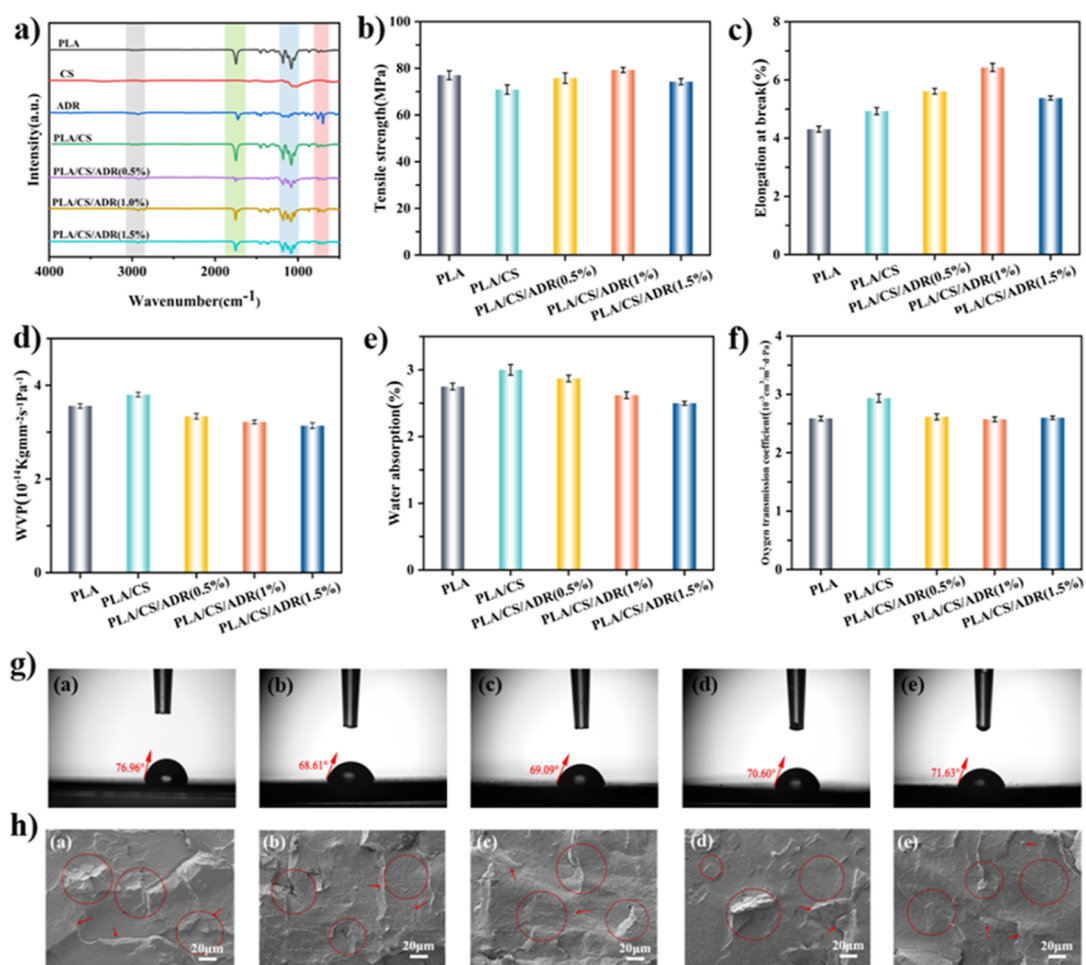


Figure 1. (a) FT-IR spectra, (b) tensile strength, (c) elongation at break, (d) WVP, (e) WA, (f) oxygen permeability coefficient, (g) contact angle test, (h) SEM images, where (a) PLA, (b) PLA/CS, (c) PLA/CS/ADR (0.5%), (d) PLA/CS/ADR (1%), (e) PLA/CS/ADR (1.5%).

relative humidity was maintained at 75%) in a crystalline dish at which time the relative humidity in the desiccator was noted as RH_1 . The desiccator was placed in a thermostat with the temperature set to 25.0 ± 0.1 °C. The mass of the glass vials was weighed and recorded at intervals of 72 h using a balance, and a graph of the change in the mass of the glass vials (m) as a function of time (T) was made, and the slope of the curve in the graph was calculated. The water vapor transmission rate (WVTR) was equal to the slope k of the curve in the graph of the calculated function divided by the area of the mouth of the glass vial, and the saturation vapor pressure (P) of water vapor at the test temperature (25 °C). The water vapor permeability (WVP) is shown in eq 2.

$$WVP = \frac{WVTR}{P(RH_1 - RH_2)} X \quad (2)$$

2.8. Oxygen Permeability Coefficient Test. Using an OX2/231 film oxygen permeability meter (Oxygen permeation meter, OX2/231, Jinan Labthink Electromechanical Co), three parallel samples of each group were placed on the oxygen permeability meter machine simultaneously for testing according to GB/T 19789–2005 requirements. After vacuuming for 3 h, the oxygen permeation coefficient test was performed, and the data were recorded.

2.9. Differential Scanning Calorimetry. The thermal properties of PLA-based composite films were investigated by

differential scanning calorimetry [differential scanning calorimeter (DSC), Diamod DSC, PerkinElmer, USA]. The heating rate was set to 10 °C/min from 20 to 200 °C and held constant at 200 °C for 10 min, then cooled from 200 to –20 °C with the cooling rate set to 10 °C/min and then from 20 to 200 °C with the heating rate set to 10 °C/min. The secondary heating curve was analyzed, and its crystallinity was calculated using eq 3.

$$X_c = \frac{\Delta H_m - \Delta H_{cc}}{\omega \times \Delta H_m} \times 100\% \quad (3)$$

ΔH_{cc} enthalpy of cold crystallization; ΔH_m enthalpy of melting; enthalpy of melting when PLA was fully crystallized, 93.7 J/g for PLA; and ω percentage of PLA-based composite film by PLA.

2.10. Dynamic Mechanical Analysis. Dynamic mechanical thermal analysis (DMA, NETZSCH, Germany) testing was performed on a DMA242 equipped with a stretching fixture, where the PLA-based composite film was ramped from 35 to 100 °C with the ramp rate set to 10 °C/min and the frequency set to 1 Hz.

2.11. Thermogravimetric Analysis. A thermogravimetric analysis (Thermogravimetric Analyzer, 209F3, NETZSCH, Germany) was used to test the thermal stability of the composite films. 5 mg of dried sample were weighed and used (upper and lower deviation was about 0.5 mg), the purge

gas used was argon, the temperature was ramped up from 30 to 500 °C, the heating rate was set to 10 °C/min, and the curve was retained for thermal stability analysis.

2.12. Scanning Electron Microscopy. The cross-sectional morphological structure of PLA-based composite films was observed by scanning electron microscopy (SEM, QUANTA 220, FEI, USA) after gold spraying of the samples with a magnification of 500 \times .

2.13. Degradation Performance Test. According to the requirements of GB/T16716.7-2012, the test samples were cut into three 50 mm \times 10 mm size in parallel for each group, weighed the mass, recorded as m_1 , and put into the compost bucket (compost bucket compost environment reference standard compost standard consists of three daily food, three rotten fruits, and special compost bran in accordance with the standard ratio, and the compost environment was kept stable for a long time). The samples were removed every 20 days, the surface was cleaned, the test mass was recorded as m_2 , the weight loss rate of composite film compost degradation was calculated, and the average value was calculated and recorded. The surface morphology of the composite was recorded using a polarized light microscope. The weight loss rate (W_d) of compost degradation was calculated according to eq 4.

$$W_d = (m_1 - m_2)/m_1 \times 100\% \quad (4)$$

2.14. Antibacterial Property. According to the GB/T31402-2015 standard, the inhibition performance of the composite material was tested by cutting the samples into 10 mm diameter discs and making three parallel samples for each group. The samples were sterilized in an electric pressure steam sterilizer with the temperature set at 120 °C for 20 min and then taken out and put into an ultraclean bench for backup. After the bacterial culture was completed, the samples were placed on its surface, put into an incubator for 24 h, and taken out, and the inhibition circle was measured to record the inhibition effect of the PLA-based composite film.

2.15. Statistical Analysis. The study recorded the average value and standard deviation of the samples. Statistical evaluation was performed using Minitab statistical software version 15, and the results were reported as mean \pm standard deviation of the replicates. All results were considered statistically significant with a p value < 0.05 .

3. RESULTS AND DISCUSSION

3.1. Basic Physical Properties of Laminated Films. The FTIR infrared spectra of pure PLA, CS, ADR, PLA/CS composite films, and PLA/CS/ADR composite films containing different proportions of ADR are shown in Figure 1a. From the figure, it can be seen that in the infrared spectrum of PLA, 2948 cm^{-1} was assigned to the stretching vibration absorption peak of the C–H bond of PLA, 1750 cm^{-1} to the stretching vibration absorption peak of the C=O bond, 1267 cm^{-1} to the stretching vibration absorption peak of the C–O–C bond and 872 cm^{-1} to the stretching vibration absorption peak of the C–C bond. In the IR spectrum of CS, 1649 cm^{-1} was attributed to the C=O stretching vibration, 1520 cm^{-1} to the N–H bending vibration, and the absorption peak at 1050 cm^{-1} to the C–O stretching vibration. The intensity of the absorption peak of the stretching vibration of the C–H bond at 2948 cm^{-1} increased with the increase in the amount of chain extender ADR, which means that more hydrogen bonds were formed, indicating a good bond between ADR and PLA. The infrared spectra of PLA/CS showed different character-

istic peaks at 1186 cm^{-1} , which was caused by the reaction of $-\text{NH}_2$ in CS with $-\text{COOH}$ in PLA to form $-\text{NH}_3^+$. The epoxy group in ADR was able to react with PLA and CS to form a C–O–C peak at 1251 cm^{-1} .

The tensile strength and elongation at break of pure PLA film, PLA/CS composite film, and PLA/CS/ADR composite film with different ADR contents are shown in Figure 1b,c, respectively. With the increase of the ADR content, the elongation at break of the PLA/CS/ADR composite film first increased to 6.43% and then decreased to 5.38%. When the ADR content was 1%, the elongation at break of the PLA/CS/ADR composite film reached a maximum value of 6.5%, which increased by 31.8% compared to 4.93% of the PLA/CS composite film, and the toughness of the composite film was improved. This was because the ADR in the PLA/CS/ADR composite film can make PLA and CS react, improve the adhesion between the PLA and CS two-phase interface, and make the composite film tougher. However, the addition of excessive ADR inhibited the movement of molecular chains in the PLA/CS/ADR composite film, and thus the elongation at break of the composite film decreased. The ADR addition ratio also has a certain effect on the tensile strength of the composite film, with the increase of ADR, the tensile strength of the composite film increases, when the amount of ADR was 1.5%, the tensile strength slightly decreased, which was due to the epoxy functional group contained in ADR. The moderate amount of ADR increases the interfacial bonding force between PLA and CS, which improves the adhesion between the matrix and the dispersed phase, but the excessive amount of ADR will have a certain obstructive effect between PLA and CS, which leads to a slight decrease in tensile strength.

The contact angle test results of pure PLA film, PLA/CS composite film, and PLA/CS/ADR composite film containing different ratios of ADR are shown in Figure 1g. As shown in the figure, the contact angle of pure PLA, PLA/CS composite film and PLA/CS/ADR composite film ranged from 68 to 76°. The contact angle gradually increased with the increase of the ADR addition ratio, and all of them were in the range of 69–72°, indicating that the hydrophobicity of the PLA/CS composite film surface could be adjusted by adding a certain amount of ADR. This was a result of the ability to better link PLAs together by the addition of ADR, which increases their chain length. The results of WA of pure PLA film, PLA/CS composite film, and PLA/CS/ADR composite film containing different amounts of ADR are shown in Figure 1e. The WA of the PLA/CS/ADR composite film decreased with the addition of ADR, when the addition of ADR was 1%, the WA rate decreased by 12.7% compared to that of the PLA/CS composite film, which was due to the addition of ADR in the composite film, the epoxy group in ADR could react with the hydroxyl and carboxyl groups of PLA, thus increasing the density of the PLA/CS/ADR composite film and thus reducing the WA rate of the composite film.

The WVTR results of pure PLA film, PLA/CS composite film, and PLA/CS/ADR composite film containing different proportions of ADR are shown in Figure 1d. With the increase of ADR content in the composite film, the WVTR coefficient of PLA/CS/ADR composite film decreased from 3.8 to 3.14, both lower than that of pure PLA and PLA/CS composite film, when the ADR content was 1.5%, the WVTR coefficient of PLA/CS/ADR (1%) composite film decreased 17.4% compared with that of PLA/CS composite film, indicating

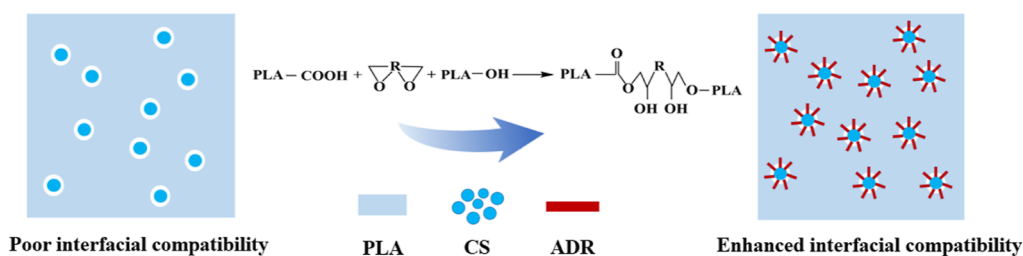


Figure 2. Modification mechanism of chain extender ADR.

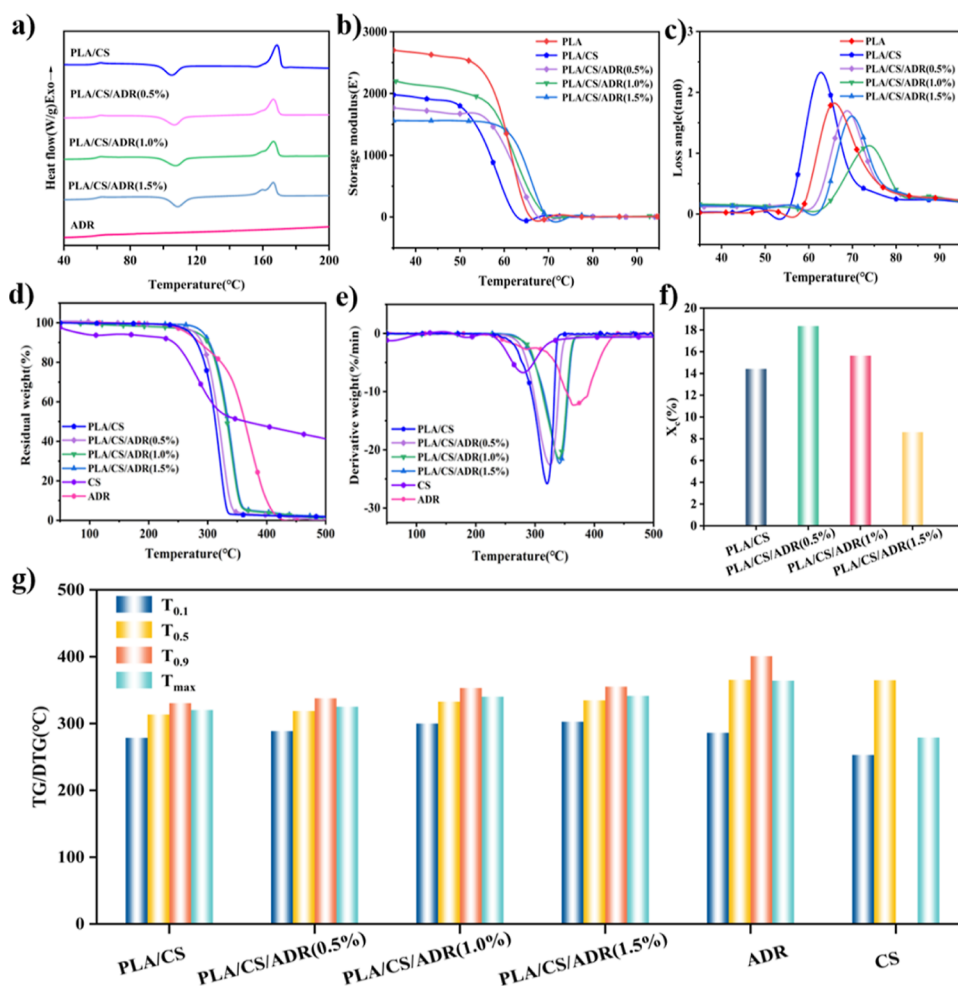


Figure 3. (a) DSC curves, (b,c) DMA curves, (d) TG curves, (e) DTG curves, (f) crystallinity curves, (g) TG/DTG curves.

that PLA/CS/ADR (1.5%) composite film has better water vapor barrier effect than PLA/CS composite film.

The oxygen transmission coefficient values of pure PLA film, PLA/CS composite film, and PLA/CS/ADR composite film containing different ratios of ADR are shown in Figure 1f. The introduction of ADR affects the oxygen permeability of PLA/CS/ADR composite films, the oxygen transmission coefficient decreases from $2.936 \times 10^{-3} \text{ cm}^3/\text{m}\cdot\text{d}\cdot\text{Pa}$ corresponding to PLA/CS composite film when different proportion of ADR was added into PLA/CS composite film, The oxygen transmission coefficient was the lowest when the ADR content was 1%, which was $2.573 \times 10^{-3} \text{ cm}^3/\text{m}\cdot\text{d}\cdot\text{Pa}$, and the oxygen transmission coefficient was the lowest at this time, indicating that the composite film has the best barrier effect on oxygen at this time. As the ADR content in the PLA/CS/ADR composite film continued to increase, the oxygen transmission coefficient

increased again to $2.599 \times 10^{-3} \text{ cm}^3/\text{m}\cdot\text{d}\cdot\text{Pa}$. This was because when the ADR content was less than 1%, the ADR weakened the intermolecular forces of PLA/CS, resulting in an intermolecular arrangement that was no longer symmetrical. When the ADR content was greater than 1%, the compatibility of PLA and CS in the composite film increased, and the molecular arrangement was no longer disordered. Overall, the oxygen permeability of the composite films did not change much after the introduction of ADR because the introduction of ADR improved the structural stability of the composite films. Once the molecular chain structure was stabilized, the increase in ADR content could not further reduce the spacing between the molecular chains, so the oxygen permeability coefficient was not obvious with the increase in ADR content.

The SEM images of pure PLA, PLA/CS composite film, and PLA/CS/ADR composite film containing different ratios of

ADR are shown in Figure 1h. Scanning electron microscope with a magnification of 500 \times , As seen in Figure 1h, the internal structure of the composite film was homogeneous, and there was no obvious separation of the two phases of PLA and CS. From Figure 1h (a), we could see the PLA as a smooth brittle fracture structure, and from Figure 1h (b), we could see the voids and cracks shown on the fracture surface of the PLA/CS composite film, as shown by the arrow in (b), it indicates that the compatibility between CS and PLA matrix was poor. As seen in Figure 1h (c–e), after the introduction of chain extender ADR in the PLA/CS composite film, CS was uniformly dispersed in PLA as the dispersed phase and showed an island structure; this indicated that the interfacial bonding between CS and PLA matrix was improved under the action of ADR, and the phase interface was more blurred, indicating that a more stable interfacial layer was formed between the two phases, and the two phases of PLA and CS were more strongly bonded. ADR can improve the toughness of PLA/CS composite film to a certain extent, and PLA and CS have good compatibility. This was because both PLA and CS molecular chains contain polar groups that interact with each other to enhance the interfacial strength and further promote the compatibility between PLA and CS. Combined with IR analysis, we could derive the modification mechanism of ADR in composite membranes (Figure 2), on the one hand, ADR connects the end groups of PLA molecular chains through ring-opening chain expansion, and on the other hand, ADR can also ring-open connect PLA and CS to enhance the compatibility.

3.2. Thermal Performance Analysis of Laminated Films. The DSC curves of PLA/CS composite films, PLA/CS/ADR composite films containing different proportions of ADR and ADR are shown in Figure 3a, The specific thermal parameters of the DSC are listed in Table 2. The DSC curve was the curve of the second heating process of the composite film, the first scan was used to eliminate the thermal history of the sample.³⁰

Table 2. Thermal Performance Data of PLA/CS Composite Film, PLA/CS/ADR Composite Film and Pure ADR

laminated film	$T_g/^\circ\text{C}$	$T_c/^\circ\text{C}$	$T_m/^\circ\text{C}$	$\Delta H_c/(\text{J/g})$	$\Delta H_m/(\text{J/g})$
PLA/CS	62.1	104.2	168.6	21.59	33.42
PLA/CS/ADR(0.5%)	61.9	106.7	166.4	14.29	30.81
PLA/CS/ADR(1.0%)	61.3	107.5	166.3	15.62	29.69
PLA/CS/ADR(1.5%)	61.1	108.8	166.1	17.32	25.07
ADR	60.7				

As seen in Figure 3a, the glass transition temperature T_g of the PLA/CS composite film was 62.1 $^\circ\text{C}$ and the melting temperature T_m was 168.6 $^\circ\text{C}$ during the temperature rise. With the addition of ADR in the PLA/CS/ADR composite film, the glass transition temperature T_g and the melting temperature T_m of the composite film both decreased to different degrees. The epoxy group contained in ADR makes PLA better connected together, and the formation of hydrogen bonds between them was accompanied by energy changes; therefore, its glass transition temperature T_g and melting temperature T_m change during the warming process. With the increasing content of ADR in PLA/CS/ADR composite films, ΔH_c increased substantially, indicating that the addition of ADR acted as a heterogeneous nucleation for PLA in PLA/

CS/ADR composite films and promoted the cold crystallization of PLA. The T_m of PLA/CS composite film and PLA/CS/ADR composite film were almost the same around 166 $^\circ\text{C}$ and T_c increased slightly with the increase of ADR, which indicates that the addition of ADR had the least effect on the melting and crystallization behavior of PLA and also shows that the introduction of ADR did not change the presence of CS in the composite film.³¹

The energy storage modulus (E') and loss angle tangent ($\tan \theta$) curves of pure PLA film, PLA/CS composite film, and PLA/CS/ADR composite film containing different proportions of ADR are shown in Figure 3b,c, respectively. As seen in Figure 3b, the storage modulus of PLA/CS/ADR composite films with different contents of ADR decreased with increasing temperature. When the ADR content was 1%, the energy storage modulus were all higher than that of the composite film without ADR addition. The energy storage modulus increased to 2202 MPa and then decreased to 1559 MPa as the ADR mass fraction increases. The loss factor of PLA/CS/ADR composite films with different levels of ADR added also showed a peak with increasing temperature. The temperature corresponding to the peak of loss angle of PLA/CS/ADR composite film increased from 66.7 to 74.1 $^\circ\text{C}$ after adding ADR to PLA/CS/ADR composite film, which shows that the glass transition temperature of PLA in PLA/CS/ADR composite film with different ADR content increased. A significant difference was found between the T_g in DSC and DMA. The T_g in DSC was related to the enthalpy change, which was a static test method with lower sensitivity, while the T_g in DMA was related to the degree of cross-linking of the polymer, which was a dynamic test method with higher sensitivity. The degree of cross-linking of the PLA/CS film increased with the addition of the ADR, resulting in an increase in the T_g in DMA.

Figure 3d,e shows the TG/DTG curves of PLA/CS films and PLA/CS/ADR composite films containing different proportions of ADR. The TG/DTG curves reflect the thermal stability of the PLA composite film, and the thermal stability parameters are $T_{0.1}$, $T_{0.5}$, $T_{0.9}$, and T_{\max} values corresponding to 10, 50, 90% weight loss and maximum degradation rate of the composite film, respectively, as shown in Figure 3g. PLA/CS/ADR composite films have relatively better thermal stability than PLA/CS composite films. With the increasing ADR content, $T_{0.1}$, $T_{0.5}$, $T_{0.9}$, and T_{\max} gradually increased, where $T_{0.1}$ gradually increased from 278.7 to 302.6 $^\circ\text{C}$, $T_{0.5}$ gradually increased from 313.5 to 334.6 $^\circ\text{C}$, $T_{0.9}$ gradually increased from 330.4 to 355.1 $^\circ\text{C}$, and T_{\max} gradually increased from 320.3 to 341.4 $^\circ\text{C}$. This indicated that the thermal stability of PLA/CS/ADR composite film gradually increases with the increase of ADR content. After the ADR reaches 1%, the decomposition temperature was basically stable, at which time the $T_{0.1}$, $T_{0.5}$, $T_{0.9}$, and T_{\max} corresponding to the PLA/CS/ADR (1%) composite film were almost unchanged compared with the corresponding values for the PLA/CS/ADR (1.5%) composite film. This was due to the increase of ADR content in the composite film within a certain range and the increase of oligomer content and amorphous phase of the composite film, and it leads to the autocatalytic cleavage of ester groups during the PLA-based pyrolysis.

Figure 3f shows the crystallinity of PLA/CS films and PLA/CS/ADR composite films containing different amounts of ADR. From the figure, the crystallinity of the films reflected a trend of increasing and then decreasing with the addition of

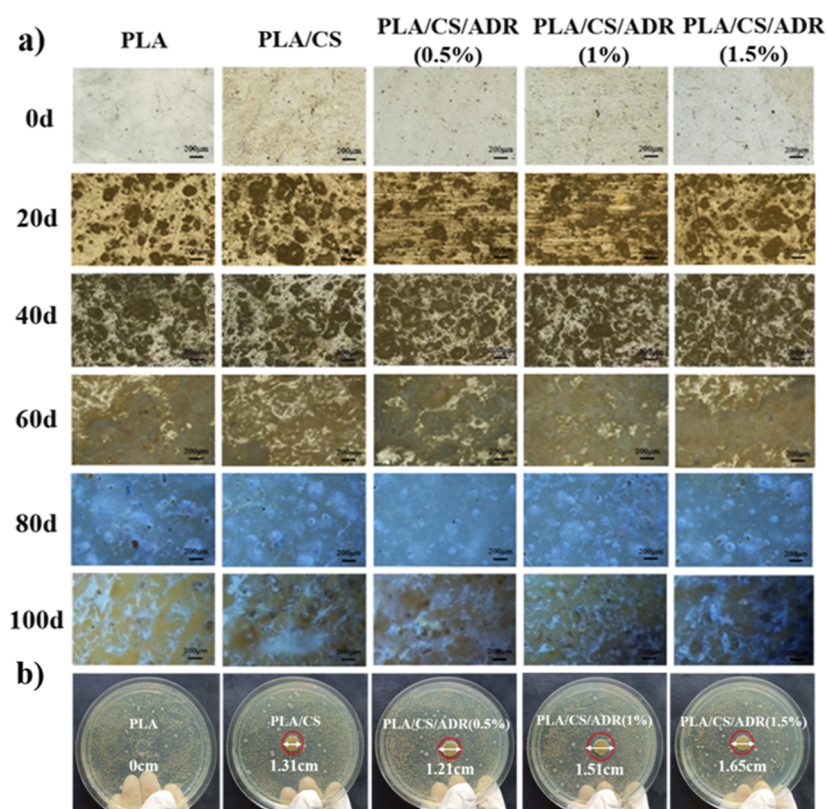


Figure 4. (a) PLA, PLA/CS composite film, and PLA/CS/ADR composite film before and after different days of composting degradation Polarized light microscope, (b) bacteria inhibition effect of PLA, PLA/CS composite film and PLA/CS/ADR composite film.

Table 3. Percentage Weight Loss of Compost Degradation for PLA, PLA/CS Composite Film, and PLA/CS/ADR Composite Film (%)

laminare film	0d/%	20d/%	40d/%	60d/%	80d/%	100d/%
PLA	0	4.41	12.55	23.46	34.82	45.86
PLA/CS	0	3.64	11.23	22.16	32.5	42.69
PLA/CS/ADR (0.5%)	0	4.02	12.01	22.93	33.71	44.27
PLA/CS/ADR (1%)	0	3.95	12.44	23.23	33.93	44.47
PLA/CS/ADR (1.5%)	0	4.11	11.97	22.54	33.44	44.17

ADR, and the PLA/CS/ADR (0.5%) composite film had the highest crystallinity, which could reach 18.36%. In general, the increase in crystallinity leads to the corresponding increase in strength, but the strength of the PLA/CS/ADR (1%) composite film was higher than that of the PLA/CS/ADR (0.5%) composite film. This was due to the fact that the 0.5% molecules were not sufficiently cross-linked, and the molecular chains were easily movable, resulting in an increase in crystallinity. However, the strength did not reach the maximum; as the concentration increased, the degree of molecular cross-linking increased and the ability of molecular movement decreased, resulting in a decrease in crystallinity, but the strength continued to increase.

As seen in Figure 4a and Table 3, the percentage weight loss from compost degradation of the composite films gradually increased as the number of degradation days continued to increase, and no significant changes were observed in the smooth surface morphology of the composite films when degradation had not started. At 20 days of degradation, the mass loss of the composite film was not much, about 4%, and during this period, it was mainly the action of microorganisms on the film that acts as a biodegradation. When degradation is

40 days, a large number of holes appear on the surface of the composite film and the holes are sunken downward and connected with other holes to form larger holes, the quality loss of the composite film begins to gradually increase and the quality was obviously reduced to about 11%, the degradation rate in this cycle was 100% faster than the previous cycle, which was due to a large number of ester bond breaks in PLA in the composite film, and the effect of ester bond breaks on the degradation quality of PLA-based composite film was significantly higher than the degradation caused by microbial decomposition and metabolism on the surface of the composite film. At 60 days of degradation, the degradation loss mass of the composite film was 22–24%, and the rate of degradation of the composite film in this cycle was about 100% higher than in the previous cycle, the surface of the composite film has become rough, and a large number of larger holes have been connected into obvious degradation areas. The degradation rate of the PLA-based composite film remained almost stable at this time. After the degradation reaches 80 days, when the degradation mass has reached about 32–34%, the surface of the composite film was rough, and in the newly formed degradation area of the previous stage, clearer white

degradation holes appear, which go down deeper and connect into gullies. In the degradation reaching 100 days, the degradation quality reached 44–45%, it was observed that the surface of the composite film was rough at this time, and the grooves appearing in the previous stage have been connected with obvious cracks, indicating that the degradation has continued to be stable at this time. In terms of degradation rate, the PLA/CS/ADR composite film has a higher degradation rate than PLA film than PLA/CS composite film, which indicates that the introduction of ADR makes PLA and CS better together and CS degrades together with the PLA matrix, while the degradation rate was relatively slow in the PLA/CS composite film without the introduction of ADR.

Bacterial inhibition tests were performed to examine the inhibition performance of pure PLA films, PLA/CS composite films, and PLA/CS/ADR composite films containing different ratios of ADR. Figure 4b shows the bacterial inhibition effect of pure PLA film, PLA/CS composite film, and PLA/CS/ADR composite film containing different ratios of ADR on *S. aureus*. As seen in Figure 4b, no inhibition circle appeared around the pure PLA film, and colonies could be observed in the area below the sample in contact with the agar, indicating that the PLA film had no inhibition effect. While in the PLA/CS composite film, the PLA/CS/ADR composite film containing different proportions of ADR showed an inhibition circle around the film, the area below the composite film in contact with the nutrient agar was free of colonies, and the bacterial colonies around the composite film were significantly reduced; the variation of the diameter of the inhibition circle can be seen in the figure. Compared with pure PLA film, PLA/CS film and PLA/CS/ADR composite film containing different proportion of ADR have certain inhibition effect, and the diameter of the inhibition circle can reach 1.3–1.6 cm in all cases.

4. CONCLUSIONS

PLA-based composite films were prepared by compression molding using the melt blending method. The properties of the composite films were analyzed, and the following conclusions were made: PLA/CS composite films were modified by using a food-grade chain extender, ADR4468, and their mechanical and other properties were investigated. It was found that after the addition of ADR4468, the carboxyl and hydroxyl groups in PLA had formed C–O–C chemical bonds by the action of ADR4468, and the mechanical properties of the PLA/CS/ADR composite film were improved. In addition, the barrier effect of the composite film to water vapor and oxygen was improved, which is beneficial for use in food packaging. From the cross-sectional morphology, it can be concluded that the phase interface between the PLA and CS matrix under the action of ADR was blurred, an interface layer was formed between the two phases, and the bonding force between PLA and CS was strong. PLA film, PLA/CS composite film, and PLA/CS/ADR composite film containing different ratios of ADR were all effectively degradable, and the raw materials used were nontoxic and harmless, which was a green and environmentally friendly process. In addition, PLA/CS laminate films and PLA/CS/ADR laminate films have antibacterial properties compared with PLA films, which was important for their use in food packaging.

AUTHOR INFORMATION

Corresponding Author

Yingjie Qiao – College of Material Science and Chemical Engineering, Harbin Engineering University, Harbin 150001, China; orcid.org/0009-0003-6976-6047; Email: qiaoyingjie2024@163.com

Authors

Tingqiang Yan – College of Material Science and Chemical Engineering, Harbin Engineering University, Harbin 150001, China

Xiaodong Wang – College of Material Science and Chemical Engineering, Harbin Engineering University, Harbin 150001, China

Complete contact information is available at:

<https://pubs.acs.org/10.1021/acsomega.4c01849>

Author Contributions

Tingqiang Yan: conceptualization, data curation, formal analysis, methodology, visualization, writing-original draft, writing-review and editing. **Xiaodong Wang**: data curation, formal analysis, methodology, validation, writing-review and editing. **Yingjie Qiao**: conceptualization, investigation, project administration, supervision, writing-review and editing.

Notes

The authors declare no competing financial interest.

ACKNOWLEDGMENTS

Financial support from the Doctoral Innovation Fund for Forestry Engineering First Class Disciplines project (LYGC202212) is gratefully acknowledged.

REFERENCES

- (1) Kerry, J. P. Chapter 23 - New Packaging Technologies, Materials and Formats for Fast-Moving Consumer Products. In *Innovations in Food Packaging (Second ed.)*; Han, J. H., Ed.; Academic Press, 2014; pp 549–584.
- (2) Cruz-Romero, M. C.; Murphy, T.; Morris, M.; Cummins, E.; Kerry, J. P. Antimicrobial activity of chitosan, organic acids and nano-sized solubilisates for potential use in smart antimicrobially-active packaging for potential food applications. *Food Control* **2013**, *34* (2), 393–397.
- (3) Abrial, H.; Basri, A.; Muhammad, F.; Fernando, Y.; Hafizulhaq, F.; Mahardika, M.; Sugiarti, E.; Sapuan, S. M.; Ilyas, R. A.; Stephane, I. A simple method for improving the properties of the sago starch films prepared by using ultrasonication treatment. *Food Hydrocolloids* **2019**, *93*, 276–283.
- (4) Zhang, Y.-R.; Zhang, S.-D.; Wang, X.-L.; Chen, R.-Y.; Wang, Y.-Z. Effect of carbonyl content on the properties of thermoplastic oxidized starch. *Carbohydr. Polym.* **2009**, *78* (1), 157–161.
- (5) Ilyas, R. A.; Sapuan, S. M.; Ishak, M. R.; Zainudin, E. S. Development and characterization of sugar palm nanocrystalline cellulose reinforced sugar palm starch bionanocomposites. *Carbohydr. Polym.* **2018**, *202*, 186–202.
- (6) Du, Y.; Wu, T.; Yan, N.; Kortschot, M. T.; Farnood, R. Fabrication and characterization of fully biodegradable natural fiber-reinforced poly(lactic acid) composites. *Compos. B Eng.* **2014**, *56*, 717–723.
- (7) Kumar, N.; Das, D. Fibrous biocomposites from nettle (*Girardinia diversifolia*) and poly(lactic acid) fibers for automotive dashboard panel application. *Compos. B Eng.* **2017**, *130*, 54–63.
- (8) Singh, N.; Hui, D.; Singh, R.; Ahuja, I. P. S.; Feo, L.; Fraternali, F. Recycling of plastic solid waste: A state of art review and future applications. *Compos. B Eng.* **2017**, *115*, 409–422.

- (9) Madhavan Nampoothiri, K.; Nair, N. R.; John, R. P. An overview of the recent developments in polylactide (PLA) research. *Bioresour. Technol.* **2010**, *101* (22), 8493–8501.
- (10) Muller, J.; González-Martínez, C.; Chiralt, A. Combination of Poly(lactic) Acid and Starch for Biodegradable Food Packaging. *Materials* **2017**, *10*, 952.
- (11) Södergård, A.; Stolt, M. Properties of lactic acid based polymers and their correlation with composition. *Prog. Polym. Sci.* **2002**, *27* (6), 1123–1163.
- (12) Syafri, E.; Sudirman; Mashadi; Yulianti, E.; Deswita; Asrofi, M.; Abrial, H.; Sapuan, S. M.; Ilyas, R. A.; Fudholi, A. Effect of sonication time on the thermal stability, moisture absorption, and biodegradation of water hyacinth (*Eichhornia crassipes*) nanocellulose-filled bengkuang (*Pachyrhizus erosus*) starch biocomposites. *J. Mater. Res. Technol.* **2019**, *8* (6), 6223–6231.
- (13) Chen, X.; Gao, S.; Yang, L.; Song, J.; Song, T.; Ling, J.; Shi, M.; Liu, J.; Wu, X.; Wang, P. Highly toughened and heat-resistant poly(l-lactide)/polyvinylidene fluoride materials through simply interfacial interaction control via epoxy chain extender. *Eur. Polym. J.* **2023**, *186*, 111839.
- (14) Elkholy, H. M.; Abdelwahab, M. A.; Naveed, M.; Abdelaziz, K.; Rabnawaz, M. Food-safe glycidyl-free chain extenders for polylactides. *Green Chem.* **2024**, *26*, 3968–3978.
- (15) Ilyas, R. A.; Sapuan, S. M.; Ishak, M. R.; Zainudin, E. S. Sugar palm nanofibrillated cellulose (*Arenga pinnata* (Wurmb.) Merr): Effect of cycles on their yield, physic-chemical, morphological and thermal behavior. *Int. J. Biol. Macromol.* **2019**, *123*, 379–388.
- (16) Sun, S.; Zhang, M.; Zhang, H.; Zhang, X. Polylactide toughening with epoxy-functionalized grafted acrylonitrile-butadiene-styrene particles. *J. Appl. Polym. Sci.* **2011**, *122* (5), 2992–2999.
- (17) Arruda, L. C.; Magaton, M.; Bretas, R. E. S.; Ueki, M. M. Influence of chain extender on mechanical, thermal and morphological properties of blown films of PLA/PBAT blends. *Polym. Test.* **2015**, *43*, 27–37.
- (18) Balart, J. F.; Fombuena, V.; Fenollar, O.; Boronat, T.; Sánchez-Nacher, L. Processing and characterization of high environmental efficiency composites based on PLA and hazelnut shell flour (HSF) with biobased plasticizers derived from epoxidized linseed oil (ELO). *Compos. B Eng.* **2016**, *86*, 168–177.
- (19) Zhou, Y.; Fan, M.; Chen, L. Interface and bonding mechanisms of plant fibre composites: An overview. *Compos. B Eng.* **2016**, *101*, 31–45.
- (20) Cheung, H.-y.; Ho, M.-p.; Lau, K.-t.; Cardona, F.; Hui, D. Natural fibre-reinforced composites for bioengineering and environmental engineering applications. *Compos. B Eng.* **2009**, *40* (7), 655–663.
- (21) Sébastien, F.; Stéphane, G.; Copinet, A.; Coma, V. Novel biodegradable films made from chitosan and poly(lactic acid) with antifungal properties against mycotoxinogen strains. *Carbohydr. Polym.* **2006**, *65* (2), 185–193.
- (22) Yu, L.; Gong, J.; Zeng, C.; Zhang, L. Synthesis of Monodisperse Zeolite A/Chitosan Hybrid Microspheres and Binderless Zeolite A Microspheres. *Ind. Eng. Chem. Res.* **2012**, *51* (5), 2299–2308.
- (23) Yu, S.-H.; Hsieh, H.-Y.; Pang, J.-C.; Tang, D.-W.; Shih, C.-M.; Tsai, M.-L.; Tsai, Y.-C.; Mi, F.-L. Active films from water-soluble chitosan/cellulose composites incorporating releasable caffeic acid for inhibition of lipid oxidation in fish oil emulsions. *Food Hydrocolloids* **2013**, *32* (1), 9–19.
- (24) Woranuch, S.; Yoksan, R. Eugenol-loaded chitosan nanoparticles: I. Thermal stability improvement of eugenol through encapsulation. *Carbohydr. Polym.* **2013**, *96* (2), 578–585.
- (25) Woranuch, S.; Yoksan, R. Eugenol-loaded chitosan nanoparticles: II. Application in bio-based plastics for active packaging. *Carbohydr. Polym.* **2013**, *96* (2), 586–592.
- (26) Fernandez-Saiz, P. 20 - Chitosan polysaccharide in food packaging applications. In *Multifunctional and Nanoreinforced Polymers for Food Packaging*; Lagarón, J.-M., Ed.; Woodhead Publishing, 2011; pp 571–593.
- (27) Liu, Z.; Ge, X.; Lu, Y.; Dong, S.; Zhao, Y.; Zeng, M. Effects of chitosan molecular weight and degree of deacetylation on the properties of gelatine-based films. *Food Hydrocolloids* **2012**, *26* (1), 311–317.
- (28) Fernández-Saiz, P.; Sánchez, G.; Soler, C.; Lagaron, J. M.; Ocio, M. J. Chitosan films for the microbiological preservation of refrigerated sole and hake fillets. *Food Control* **2013**, *34* (1), 61–68.
- (29) Bie, P.; Liu, P.; Yu, L.; Li, X.; Chen, L.; Xie, F. The properties of antimicrobial films derived from poly(lactic acid)/starch/chitosan blended matrix. *Carbohydr. Polym.* **2013**, *98* (1), 959–966.
- (30) Pracella, M.; Haque, M. M.-U.; Puglia, D. Morphology and properties tuning of PLA/cellulose nanocrystals bio-nanocomposites by means of reactive functionalization and blending with PVAc. *Polymer* **2014**, *55* (16), 3720–3728.
- (31) Elsawy, M. A.; Saad, G. R.; Sayed, A. M. Mechanical, thermal, and dielectric properties of poly(lactic acid)/chitosan nanocomposites. *Polym. Eng. Sci.* **2016**, *56* (9), 987–994.